

See discussions, stats, and author profiles for this publication at: <https://www.researchgate.net/publication/221721739>

# Molecular Modeling of the Structural and Dynamical Properties of Secondary Plant Cell Walls: Influence of Lignin Chemistry

ARTICLE in THE JOURNAL OF PHYSICAL CHEMISTRY B · MARCH 2012

Impact Factor: 3.3 · DOI: 10.1021/jp300395k · Source: PubMed

---

CITATIONS

10

READS

56

---

## 2 AUTHORS:



Landry Charlier

Université de Montpellier

15 PUBLICATIONS 108 CITATIONS

[SEE PROFILE](#)



Karim Mazeau

University Joseph Fourier - Grenoble 1

93 PUBLICATIONS 1,998 CITATIONS

[SEE PROFILE](#)

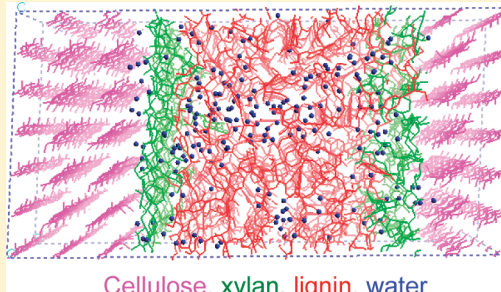
# Molecular Modeling of the Structural and Dynamical Properties of Secondary Plant Cell Walls: Influence of Lignin Chemistry

Landry Charlier and Karim Mazeau\*

Centre de Recherches sur les Macromolécules Végétales (CERMAV-CNRS) (affiliated with the Université Joseph Fourier and member of the Institut de Chimie Moléculaire de Grenoble), BP 53, F-38041 Grenoble cedex 9, France

Supporting Information

**ABSTRACT:** A modeling of lignified secondary plant cell walls adapted to grass has been achieved, using molecular dynamics for time up to 180 ns, applied to systems composed of cellulose, xylan, water, and lignin. The overall model, which was 70 nm thick for a volume of 74.4 nm<sup>3</sup>, consisted of two crystalline cellulose layers, each being two molecules deep, separated by an interlayer space where the three other components were located. Whereas the cellulose and xylan chemistry was fixed, 18 lignin systems were considered that varied not only in guaiacyl, syringyl, and *p*-hydroxyphenyl composition, but also in chain length, linkage types, and the presence or absence of coumaryl units. The stabilized models showed a well-defined interface between xylan and cellulose, but some interpenetration of xylan into the lignin part of the models. A survey of the 18 models showed that their lignin component was amorphous and that their density profile was very variable and essentially model dependent. This variability was also reflected in the co-orientation of the lignin phenyl rings with respect to the cellulose surfaces, some systems showing some orientation whereas others did not. The pattern of void distribution accessible to water varied from one system to the next, but the overall void volume was systematically established at around 3%, accepting around 200 water molecules. The estimated mobility of the water molecules interacting with lignin was 1.5 times greater than that interacting with carbohydrates.



Cellulose, xylan, lignin, water

## I. INTRODUCTION

It is commonly accepted that biofuel will be of more importance in the future to replace the dwindling fossil fuel reserves.<sup>1</sup> To date, a substantial amount of biofuel comes from bioethanol, which results from the fermentation of starch—either from corn or wheat—or of the single sugar sucrose from sugar cane or sugar beet. Despite its current commercialization, it seems that such a “first-generation” biofuel has a limited future since its production competes directly with that of the food that is required to feed the expanding world population.<sup>1</sup> Lignocellulosic products and byproducts, either from agricultural waste or from plants growing on poor soil, do not enter in the “food-versus-fuel” debate. They are therefore the logical target for manufacturing “second-generation” biofuel from the fermentation of the carbohydrates that constitute the major part of lignocellulosics.<sup>2</sup>

Most of the plant material that would be available for biofuel production comes from secondary lignified cell walls of plants, either from wood or grass-related plants. Besides variations, depending on the plant categories, the commonly accepted secondary cell-wall model is based on a layer-like superposition of three components:<sup>3–7</sup> (i) a distribution of crystalline cellulose microfibrils, which constitute from 40 to 50% of the wall dry weight,<sup>2</sup> (ii) hemicelluloses that are partially adsorbed onto the microfibril surfaces, and (iii) lignin, acting as a glue linking the microfibril/hemicellulose components, and partly hooked to the hemicellulose by so-called “lignin carbohydrate

complexes (LCCs).<sup>8</sup> While the knowledge of the structure and ultrastructure of cellulose in the cell walls is fairly well established, less is known about the organization of the hemicelluloses, and still much less on the lignin ultrastructure. Indeed, when comparing hemicelluloses with lignin, the former essentially consists of linear molecules that can be extracted and characterized, whereas the latter is a three-dimensional (3D) intractable polymer where the building blocks are connected to one another in numerous ways by aryl ether bonds of the  $\beta$ -O-4 linkage type together with carbon–carbon bonds. Lignin, which occurs at a later stage in the developing cell wall, results from the association of three monolignol precursors differing in their degree of methoxylation. When polymerized and reticulated in three dimensions, these precursors yield lignins that can be characterized as composed of *p*-hydroxyphenyl (H), guaiacyl (G) and syringyl (S) phenylpropanoid units.<sup>9</sup> In most hardwoods, lignin consists of G and S units together with traces of H. On the other hand, in softwood, lignin contains essentially G units and a low level of H. In grasses, lignin resembles that of hardwood, except that there are more H components together with some paracoumaryl and ferulate units.<sup>9</sup>

**Received:** January 12, 2012

**Revised:** March 15, 2012

**Published:** March 19, 2012

Lignin, being polyaromatic and rather hydrophobic, presents an inherent resistance to chemical and biochemical attack. Thus, lignin acts as an effective barrier to avoid plant attacks by fungi and insects. As an inevitable corollary, lignin also behaves as a substantial obstacle for the hydrolysis and digestion of the cell wall polysaccharides into fermentable sugars. Besides this general concept, it seems that there are important variations in the degradability of plant cell walls depending on the lignin composition and chemistry. At first, the ratio G/S has been suggested as a determinant factor. This is best illustrated by considering the degradability of the plant cell wall of a given species, when the G/S ratio, together with the lignin content, was varied by genetic engineering or phenotype selection. In the case of *Populus*, a low S/G ratio, together with a low lignin content led to a substantial increase in the release of xylose upon acid hydrolysis.<sup>10,11</sup> That observation was corroborated in transgenic tobacco,<sup>12</sup> alfalfa,<sup>13</sup> and *Arabidopsis*,<sup>14</sup> but a reverse effect, which points toward a more complex situation, was found in the lignin of recombinant maize.<sup>15,16</sup> These contradictory results indicate that, beyond the S/G ratios and lignin content, the inherent chemical structure of lignin and its 3D organization may play determinant parts in the ease of the degradability of the plant cell wall. Features such as lignin porosity, distribution of the linkages, number of branching points, interconnection of lignin and hemicelluloses, together with hydrogen bonding and hydration possibility seem to be of importance. Unfortunately, most of the analytical methods that are used to describe lignin rely on chemical depolymerization, followed by extraction and characterization of lignin fragments. From these, it appears nearly impossible to reconstitute the 3D cross-linked organization of lignin from the chemical analysis of its fragments and thus to propose an elaborate molecular model of the secondary plant cell wall.

With the failure of traditional analytical techniques, modeling appears as a promising approach to describe the structure and ultrastructure of lignin in its cell wall environment. Indeed, modeling is able to provide stable 3D representations at the atomic scale, not only of the extracted lignin fragments, but also of the *in situ* components. Molecular modeling of isolated dimers<sup>17–20</sup> and oligomers<sup>21–23</sup> of lignin have revealed the intrinsic conformational properties of the different lignin linkages, showing models that are well supported by X-ray crystallography and NMR data.<sup>24–26</sup> Simulations of lignins in aqueous environment have shown the temperature dependence of such biphasic systems.<sup>27</sup> Models of lignin associated with cellulose have been proposed.<sup>28–31</sup> These calculated models have shown that the plane of the phenyl rings of lignin had a tendency to be aligned parallel to the cell wall surfaces, in agreement with data resulting from Raman microprobe studies.<sup>32</sup> Other models, which have focused on the lignin–water interactions, have described the mobility of water in terms of methoxyl number in the system.<sup>33</sup> So far, the full association of cellulose, hemicellulose, lignin, and water has been difficult to model due to the complexity of such a four-component system. In one attempt based on quantum mechanics methods, the authors had to oversimplify the problem by considering mono- and disaccharides and their association with the basic structural elements of lignin.<sup>34</sup> In another report, Faulon et al. relied on empirical potential methods based on energy minimization and molecular dynamics (MD) to describe the structure of the gymnosperm secondary wall.<sup>35</sup> Unexpectedly, the outcome of their study was the proposal of a regular helical model for lignin that

contradicts the current belief, indicating that cell wall lignin must be essentially amorphous and therefore aperiodic. It must be noted that in their study, Faulon et al. used several shortcuts. In particular, they modeled the adsorption of hemicellulose on the elusive (010) surface of cellulose crystalline microfibrils, instead of the (110) and ( $\overline{1}10$ ) surfaces, which are normally expected.<sup>36</sup> Furthermore, they also achieved their study under “vacuum conditions”, which do not take into account the hydrogen bonding capability of water molecules that are believed to be present throughout the cell wall. Given these conditions, we feel that the helical model of lignin should be taken with care. Indeed, it is likely that the hydration possibilities and the choice of other cellulose surfaces for the adsorption of hemicelluloses should have a substantial impact on the ultrastructural organization of the cell wall. For these reasons, we have built models of secondary plant cell wall by sequentially adding cellulose, hemicellulose, lignin, and water within a given periodic parallelepipedic box, mimicking the basic layer of the multilayered cell wall. This report describes the construction of these models and their outcome after MD simulations over periods of several nanoseconds.

## II. MATERIALS AND METHODS

In this study, we have used the modeling software Cerius2 (Accelrys Inc., San Diego, CA, USA) for the construction of the initial systems, and Gromacs v.4.5.3 for the simulations.<sup>37</sup> These programs were run on workstations connected to the “Centre d’Expérimentation et de Calcul Intensif”, CECIC, Grenoble, France.

The strategy for construction of the cell wall models followed a “bottom-up” approach, whereby cellulose was generated first, followed by the generation of the cellulose/hemicellulose complex, which was then sequentially ferulated, lignified, and hydrated.

**Cellulose Model.** The coordinates of the crystal structure of I $\beta$  cellulose derived from X-ray and neutron diffraction data were used.<sup>38</sup> These coordinates were used to build a periodic super crystal of cellulose made of 24 cellulose chains having the (110) and ( $\overline{1}10$ ) crystallographic planes parallel to the BC and AC surfaces of the supercell, respectively. Each cellulose chain contains six glucosyl residues and is covalently bonded across the periodic supercell in order to model an infinite chain. The super crystal was then subjected to an equilibration step, using NPT MD, at 300 K and 1 atm.<sup>39</sup> It must be noted that the NPT equilibrated values of the cell parameters deviates slightly from those derived from X-ray crystallography data. A model of two crystalline layers of equilibrated cellulose, two molecules deep, exposing the (110) crystallographic planes, was then built by manually increasing the *B* parameter of the supercell, each layer (12 cellulose chains each) being separated by an interlayer spacer (Figure 1). The working model was thus a parallelepiped defined by *A*, *B*, and *C* sides together with angles  $\alpha$ ,  $\beta$ , and  $\gamma$ . The parameters *A* and *C* and the three angles are connected to the equilibrated unit cell of cellulose I $\beta$ . The values were *A* = 3.05 nm, *C* = 3.49 nm,  $\alpha$  = 90°,  $\beta$  = 90° and  $\gamma$  = 92.6°. *B*, being the overall thickness of the model, is therefore the sum of the thickness of the two layers of cellulose and that of the interlayer spacer where the other cell wall components were inserted during the model building (see below).

**Hemicelluloses.** Only hemicelluloses of the xylan type were considered in this study. The modeled fragments consisted of 16 D-xylopyranosyl residues, connected linearly by (1→4)- $\beta$ -type linkages and regularly substituted by three L-Arabinofur-

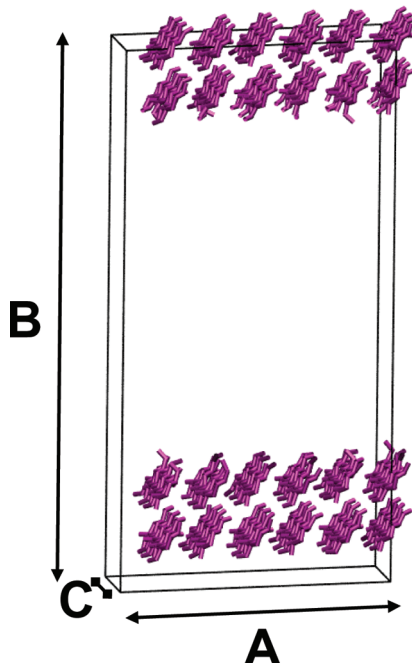


**Figure 1.** Schematic representation of the cellulose model. The lattice of cellulose chains in purple color is seen in the cross section perpendicular to the parameter C.

anoyl (Araf) linked  $\alpha$ -(1 $\rightarrow$ 3) to the xylosyl residues. These fragments can be defined as  $X_3AX_4AX_4AX_2$ , according to the recently proposed nomenclature.<sup>40</sup> Each model contained four of these xylan fragments, two of them per cellulose surface.

The generation of the cellulose xylan complex was performed according to the procedure described in earlier work.<sup>41</sup> In short, the xylan fragments were sequentially inserted within the model next to each cellulose surface, in a random orientation and in an unperturbed conformation.<sup>42</sup> Their adsorption on cellulose was performed thanks to a combination of energy minimization and MD.

**Ferulate.** One ferulate moiety (see Figure 2A) in the “a” and “c” models and two moieties in the “b” model (see below) were then added to the xylan chains of each cellulose/hemicellulose complex. Each ferulate was covalently bound to an arbitrarily selected, but solvent-exposed Araf of the xylan chains. The stable conformations of the ferulate moiety of the hemicellulose/cellulose complex were established by coupling Monte Carlo procedures, and assigning random values to the five torsion angles (T1–T5 in Figure 2) of the ferulate group, followed by energy minimization. For each added ferulate bridge, 5000 conformations were generated. One of them was selected according to its total potential energy and the degree of exposure to the first lignin residue. A minimum energy was necessary to ensure that the generated model was stable, and a significant exposure of the first lignin unit was required in order to facilitate the addition of the lignin fragments.

**Lignin.** Lignin is characterized by a wide variety of chemical structures and linkages classified as H, G, and S units.<sup>43</sup> We have generated and incorporated in the Gromos 53a6 force field a library of monomers and of intermonomers linkages (files can be provided upon request).

Using this library, it is thus possible to generate any fragment of lignin with a total control of (i) its degree of polymerization (DP), (ii) its amount and sequence in H, G, and S units, (iii) its percentage and sequence of interunit linkages 5–5, 4–O–5,

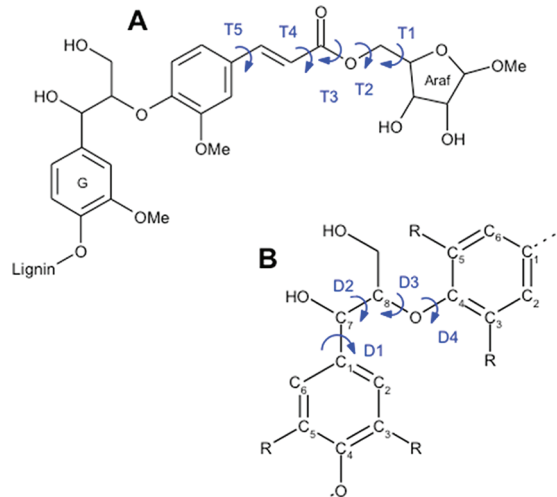


**Figure 2.** (A) The ferulate bridge between an Araf of the hemicellulose chain and the first unit of lignin (guaiacyl in the figure). (B) The  $\beta$ -O-4 linkage. Key torsion angles are indicated as D1–D4 in Figure 2B, where D1 is defined as C8–C7–C1–C2, D2 is O4–C8–C7–C1, D3 is C4–O4–C8–C7, and D4 is C3–C4–O4–C8.

$\beta$ -5,  $\beta$ -O-4,  $\beta$ -1,  $\beta$ - $\beta$ . Eighteen lignin models were considered in this study (Table 1). They were based on variations of six families, namely, GBO4, consisting of guaiacyl units linked in  $\beta$ -O-4, SBO4, consisting of syringyl units linked in  $\beta$ -O-4, SW, corresponding to softwood lignin, HW, corresponding to hardwood lignin, SBO4coum, identical to SBO4 but coumarylated, and HWcoum, identical to HW but coumarylated. In each model, the lignin molecular weight was kept constant at a value of around 22 000 g·mol<sup>-1</sup>. In each of the six families, a variation of three models was built: in the “a” models, there were two long chains; in the “b” there were four short lignin chains, and in the “c” there were two short chains, each of them being twice branched with other short chains. Note that we do not attempt to model real chemical structures of lignin, even though some models were quoted as belonging to the hardwood or softwood categories.

To avoid steric clashes that may arise during the insertion of the lignin model, the dimension B of the periodic box perpendicular to the surfaces was considerably enlarged, typically up to 30–50 nm. Fragments of lignin, which were then covalently linked to the ferulate group, were inserted in the simulation medium. Then several compression cycles followed by relaxation were performed following a protocol described in detail by Henao et al.<sup>44</sup>

This procedure allowed generating a collection of models differing in their B parameter, which varied as a function of the spacing between the cellulose surfaces.  $B_{eq}$  was defined as the B parameter for which the potential energy of the structure was minimal during the compression step. Since all the values of  $B_{eq}$  were around 7 nm, the presented structures were defined with a B value of exactly 7 nm, yielding a volume of 74.4 nm<sup>3</sup> for the model. Two compression simulations were performed for each lignin model, differing only in the initial velocity applied to the unconstrained atoms. The results were reproducible, and the data presented in this study were averaged.

**Water.** The ultimate step in the generation of the plant cell wall model consisted of adding explicit simple point charge (SPC) water molecules<sup>45</sup> in the voids of the cellulose/hemicellulose/ferulate/lignin models.

**Table 1. Composition in Percentages of the Basic Units of the 18 Lignin Systems Considered in This Work: (H) Parahydroxphenyl, (G) Guaiacyl, and (S) Syringyl Units<sup>a</sup>**

		H	G	S	Coum	5–5	4–O–5	β–S	β–O–4	β–1	β–β
GBO4	a	0	100	0	0	0	0	0	100	0	0
	b	0	100	0	0	0	0	0	100	0	0
	c	0	100	0	0	2	2	0	96	0	0
SBO4	a	0	0	100	0	0	0	0	100	0	0
	b	0	0	100	0	0	0	0	100	0	0
	c	0	6	94	0	0	2	2	96	0	0
SW	a	4	96	0	0	20	2	10	48	13	7
	b	4	96	0	0	19	2	10	50	13	6
	c	3	98	0	0	20	3	10	48	13	7
HW	a	0	48	52	0	4	3	3	84	4	3
	b	0	48	52	0	3	3	3	85	3	3
	c	0	50	50	0	6	3	3	82	4	4
SBO4coum	a	0	0	100	24	0	0	0	100	0	0
	b	0	0	100	25	0	0	0	100	0	0
	c	0	7	93	24	2	2	0	95	0	0
HWcoum	a	0	50	50	25	4	4	4	79	4	4
	b	0	49	51	25	4	4	4	80	3	3
	c	0	49	51	24	6	5	3	77	4	4

<sup>a</sup>The suffix “Coul” is used to indicate the percentage of S coumarylated units. The percentages of 5–5, 4–O–5, β–S, β–O–4, β–1, and β–β type of interunit linkages are also given. (a) Model having two lignin chains of DP 60. (b) Model having four lignin chains of DP 30. (c) Model including a branching point.

**Final Model.** The full model was then energy minimized and slowly heated by MD simulation from 0 to 300 K over a period of 15 ps. The MD was then continued for 35 ps in order to stabilize the temperature and energies. After this equilibration step, a simulation of 10 ns was started, and the statistical sampling generated was used to calculate the different average properties. In these simulations, the positions of ring atoms of the cellulose glucopyranose were kept fixed in a frozen position, while all the other atoms were free to move.

**Computational Details.** The Gromos53a6 force field was used.<sup>46</sup> The minimization uses the steepest descent and conjugate gradient algorithms, this process being stopped once the convergence criterion of 10 kJ·mol<sup>-1</sup>·nm<sup>-1</sup> is obtained. The MD simulations were performed in the canonical NVT ensemble (with constant number of particles, volume, and temperature). The equations of motion were solved using the leapfrog algorithm<sup>47</sup> with time steps of 1 fs. The system was coupled to a bath at 300 K using the velocity (*v*) rescale algorithm.<sup>48</sup> The electrostatic potential was estimated by the particle mesh Ewald (PME) algorithm,<sup>49,50</sup> with a cutoff of 0.9 nm.

**Density Profiles.** The density profiles of each component of the plant cell wall models were calculated along an axis normal to the surface of cellulose. The profiles were deduced from the last 2 ns of the MD trajectories by considering layers of 0.5 Å thickness.

**Detection of the Hydrogen Bonds.** The presence of a hydrogen bond was geometrically detected by a maximal hydrogen–oxygen distance of 0.25 nm and a minimal oxygen–hydrogen–oxygen angle of 135°.

We differentiated the water molecules, which spent less than 20% of the total 10 ns time near the lignin atoms or near those of the carbohydrates, either from cellulose or hemicellulose. These water molecules are named “water carbohydrate group” or “water lignin group”, respectively. A distance lower than or equal to 0.4 nm between the gravity center of the water molecule and any atom of either the lignin or the carbohydrate

moieties was selected as the criterion used to assess the proximity. Such water molecules will hereafter be called “isolated” from the other water molecules; in contrast, all the nonisolated water molecules will be considered to belong to an aggregate of water molecules.

**Diffusion Coefficients of the Water Molecules.** The diffusion coefficient of the water molecules in the models was calculated from the slope of the mean-square displacement for long times; at these times Einstein diffusion is observed, and the mean-square displacement is a linear function of time:

$$D = \frac{1}{6} \lim \frac{d}{dt} (\mathbf{r}(t) - \mathbf{r}(0))^2$$

where *D* is the diffusion constant, *t* is time,  $\mathbf{r}(t)$  is the position vector of the water molecules at time *t*, and the ensemble average is obtained from averaging over all water molecules (or those water molecules of the sugar group or lignin group) and all time origins. This equation only applies in the limit of large times, times at which the simulated water molecules have performed enough jumps for their trajectories to become a random walk in the plant cell wall model.

## RESULTS

The main features of the 18 plant cell wall models that were considered and described in Table 1, are reported in Tables 2 and 3. Table 2 gives a selection of some characteristics of each of these systems: the amount of water in terms of number of water molecules, the void volume, the final interaction, and potential energies. Remarkably, this table indicates that despite substantial variation in the chemical structure of the various lignin systems, the values of the different parameters that are listed in Table 2 are not so different. Table 3 focuses on the hydrogen bonding characteristics of the lignin components, either resulting from lignin-to-lignin interaction or water to lignin. As in the case of the data in Table 2, there is only a little difference in the values that are listed in Table 3, when going from one lignin system to the next.

**Table 2. Selected Characteristics of the Plant Cell Wall Models<sup>a</sup>**

		$N_{H_2O}$	void	$E_{tot}$	$E_{inter}$
GBO4	a	201	3.17	5.708	-205.0
	b	196	3.11	5.688	-206.3
	c	192	3.05	5.770	-214.9
SBO4	a	196	3.41	5.803	-200.9
	b	187	3.09	5.821	-172.9
	c	191	3.18	5.829	-182.7
SW	a	210	3.52	4.886	-208.9
	b	202	3.31	5.338	-171.0
	c	198	3.06	5.459	-200.0
HW	a	203	3.36	5.641	-197.6
	b	189	2.76	5.688	-181.8
	c	191	2.98	5.739	-188.2
SBO4coum	a	195	3.23	5.443	-193.9
	b	179	2.89	5.489	-182.5
	c	182	2.94	5.500	-198.8
HWcoum	a	197	2.91	5.465	-182.4
	b	198	3.03	5.440	-174.6
	c	203	3.33	5.465	-186.8

<sup>a</sup> $N_{H_2O}$ : number of water molecules. void: average void volume ( $\text{nm}^3$ ).

$E_{tot}$ : total energy at the end of the 10 ns of MD ( $\times 10^4 \text{ J}\cdot\text{mol}^{-1}$ ).  $E_{inter}$ : interaction energy between lignin and the carbohydrate fraction ( $\times 10^4 \text{ J}\cdot\text{mol}^{-1}$ ). Typical standard deviations are 15 for  $N_{H_2O}$ , 0.2  $\text{nm}^3$  for void,  $0.15 \times 10^4 \text{ J}\cdot\text{mol}^{-1}$  for  $E_{tot}$ , and  $16 \times 10^4 \text{ J}\cdot\text{mol}^{-1}$  for  $E_{inter}$ .

Figure 3A gives a graphical representation of one of the systems: the GBO4-a, defined in Table 1, as having two long lignin chains and consisting exclusively of guaiacyl units connected with  $\beta-\text{O}-4$  linkages.

In Figure 3A, the hydrated lignin component, which occupies the center of the parallelepiped, is surrounded by two cellulose layers coated at their surface by hemicelluloses. In the full cell wall model, the parallelepiped is periodically repeated in a multilayer system in the direction perpendicular to the cellulose surface and infinitely in the parallel directions.

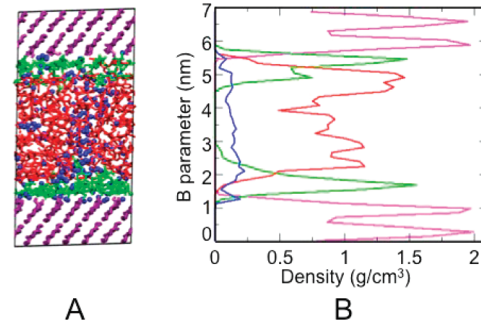


**Figure 3. (A)** A/B projection of the equilibrated GBO4-a model. The hydrogen atoms are omitted for clarity. **(B)** Density profiles calculated along B. Cellulose is colored in purple, xylan in green, lignin in red, and water in blue.

Figure 3B gives the density profiles of the different constituents of the same system, calculated along the axis normal to the cellulose surfaces (B parameter). This profile, together with the visual inspection of Figure 3A, reveals the distribution and the organization of the various species in the model.

The density profile of the cellulose component (purple) shows four intense peaks, two on each side of the figure: they correspond to the two cellulose layers in their crystalline organization, the thickness of each layer being about 1 nm. As aforementioned, in order to save computation time, the constraints applied to the atoms of the glucopyranose rings of cellulose impose to the cellulose layers their original organization. This restriction appears justified, as in a preceding study, the cellulose, which was free to adjust its conformation and organization, experienced only reorganization of its surface hydroxyl and hydroxymethyl groups, but the chair form of the glucopyranose rings was preserved.<sup>51</sup> In Figure 3B, the density profile of the cellulose surfaces overlaps with those of the other molecular species. A survey of this overlap indicates that the cellulose surfaces interact strongly with xylan and more weakly with lignin and water.

**Table 3. Description of the Hydrogen Bonds: Number of Donor and Acceptor Groups and Number of Hydrogen Bonds<sup>a</sup>**

	LL				LW				
	donor number	acceptor number	H-bonds number	sd	donor number	acceptor number	H-bonds number	sd	
GBO4	a	222	440	67.5	4.95	624	641	148.0	7.07
	b	220	432	68.5	0.71	612	628	127.5	3.54
	c	218	436	73.0	2.83	601	627.5	130.0	1.41
SBO4	a	192	475	71.0	8.49	584	671	117.5	0.71
	b	192	470	70.5	6.36	565	656.5	124.5	9.19
	c	190	471	75.0	4.24	571	661.5	115.5	7.78
SW	a	210	411	61.0	1.41	630	621	123.5	16.26
	b	209	405	65.0	0.00	612	606.5	120.0	12.73
	c	208	411	60.5	3.54	604	609	137.0	5.66
HW	a	198	453	63.5	0.71	604	656	130.0	2.83
	b	196	446	63.5	2.12	573	634.5	128.0	4.24
	c	198	451	63.0	4.24	579	641.5	129.0	7.07
SBO4coum	a	166	450	62.0	1.41	556	645	111.5	7.78
	b	166	445	64.0	11.31	523	623.5	103.0	15.56
	c	166	449	66.0	2.83	530	631	118.5	2.12
HWcoum	a	178	436	63.0	7.07	572	633	130.5	26.16
	b	175	428	64.5	2.12	570	625.5	116.0	8.49
	c	177	436	62.0	0.00	582	638.5	120.5	2.12

<sup>a</sup>LL: lignin to lignin H-bonds. LW: lignin to water H-bonds. sd: standard deviations. a, b, and c are defined as in Table 1.

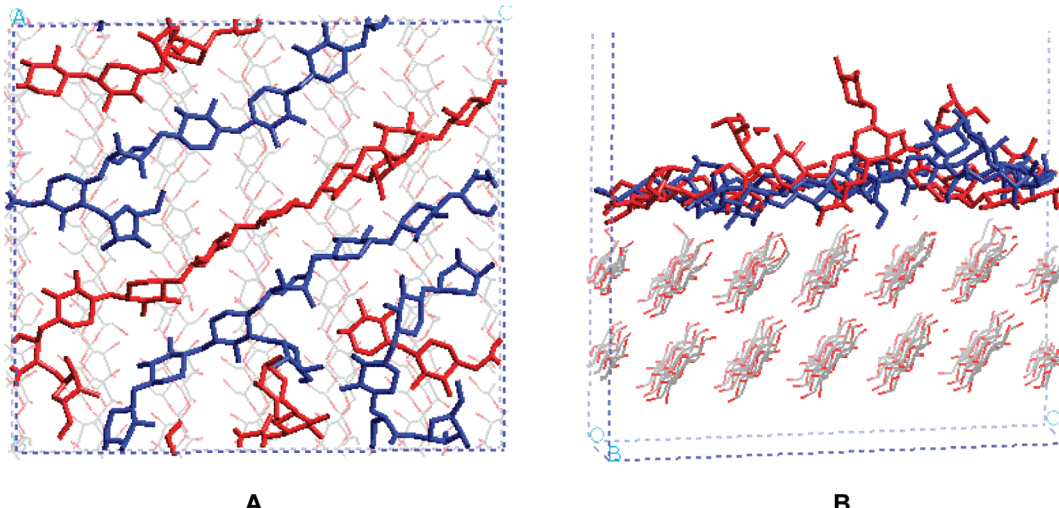


**Figure 4.** Xylan adsorbed as a monomolecular film on a cellulose surface with vertical cellulose chain axis in the model GBO4-a. (A) projection parallel to the cellulose surface. (B) Projection perpendicular to the cellulose surface.

The density trace of xylan (green line) shows a major peak at each interface with cellulose and either a less intense second peak or simply a shoulder at the interfaces with lignin, indicating therefore that the covering of the cellulose surface is somewhat larger than that of the monolayer (see Figure 3). On the other hand, the densities of xylan and lignin overlap over more than 1 nm, which is the signature of a substantial interpenetration of the two moieties. Besides this overlap, the profile of the density of lignin (red line) displays a strong fluctuation, indicating an inhomogeneous distribution of lignin within the model. The density of water (blue line) is more or less constant in between the two cellulose layers, which are impermeable to water, but this is not the case for hemicelluloses and lignin, which are permeated more or less evenly with water.

Further details of the association of the xylan chains with respect to cellulose are presented in Figure 4. As in an earlier report,<sup>41</sup> where we have extensively discussed this association, the xylan chains adopt an extended conformation when they are adsorbed on cellulose. In addition, they are roughly aligned with respect to one another, even though some imperfections can be observed (Figure 4A). On the other hand, the xylan chains are not aligned parallel to the cellulose fiber axis. In cross section (Figure 4B), one sees that most of the xylan molecules are laid flat on the cellulose surface, but for some of them, there are a few segments that have a tendency to migrate toward the lignin components.

Figure 5 illustrates, in superposition, the density profiles of xylan, lignin, and water for the three systems of the GBO4 family: GBO4-a, already seen in Figure 4, GBO4-b, and GBO4-c. The remaining 15 profiles that are also considered in this work are presented in the Supporting Information, Figure S2). As seen in Figure 5, the density profiles of xylan and water fractions seem insensitive to the chemistry of the lignin system. Indeed, in the figure, the densities of these components, which are drawn through the thickness of the model, are nearly superimposable. The lignin density was not uniform, as it showed high fluctuations around a mean density of  $1 \text{ g}\cdot\text{cm}^{-3}$ . This observation revealed the inhomogeneous distribution of lignin in the model, with zones of high density coexisting with zones of low density. Thus, a characteristic of this fluctuation is that it appears to be strongly model-dependent. This is clearly

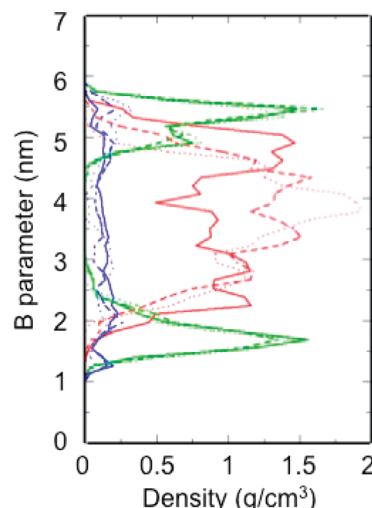


**Figure 5.** Superimposition of the density profiles of the three GBO4 models. GBO4-a (two long lignin chains): continuous line; GBO4-b (four short lignin chains): dotted line; GBO4-c (short lignin chains with two branching points): dashed line. The density of the cellulose component has been omitted. Xylan is colored in green, lignin in red, and water in blue.

seen in comparing, for instance, the lignin density of GBO4-a and that of GBO4-b at the center of the model, where the GBO4-a presents a minimum, whereas the density is at its maximum for GBO4-b.

Figure 6 shows the angular domains explored by the D1, D2, D3, and D4 torsion angles of the dominant  $\beta$ -O-4 linkages defined in Figure 2. In this figure, the distribution of the angular population is given for the six lignin families that are described in Table 1. Remarkably, for the three angles D1, D2, and D3, the angular distribution is nearly identical when going from one family to the next. The dihedral angle D1 explores two large torsion spaces, +g (angular domain from  $30^\circ$  to  $+90^\circ$ ) and -g (angular domain from  $-30^\circ$  to  $-90^\circ$ ), which are roughly of similar importance. The angle D2 explores almost the whole angular space, although the +g orientation is more explored. In contrast, the torsion angle D3 explores mostly a single region, which is nevertheless very large, ranging from -g to trans

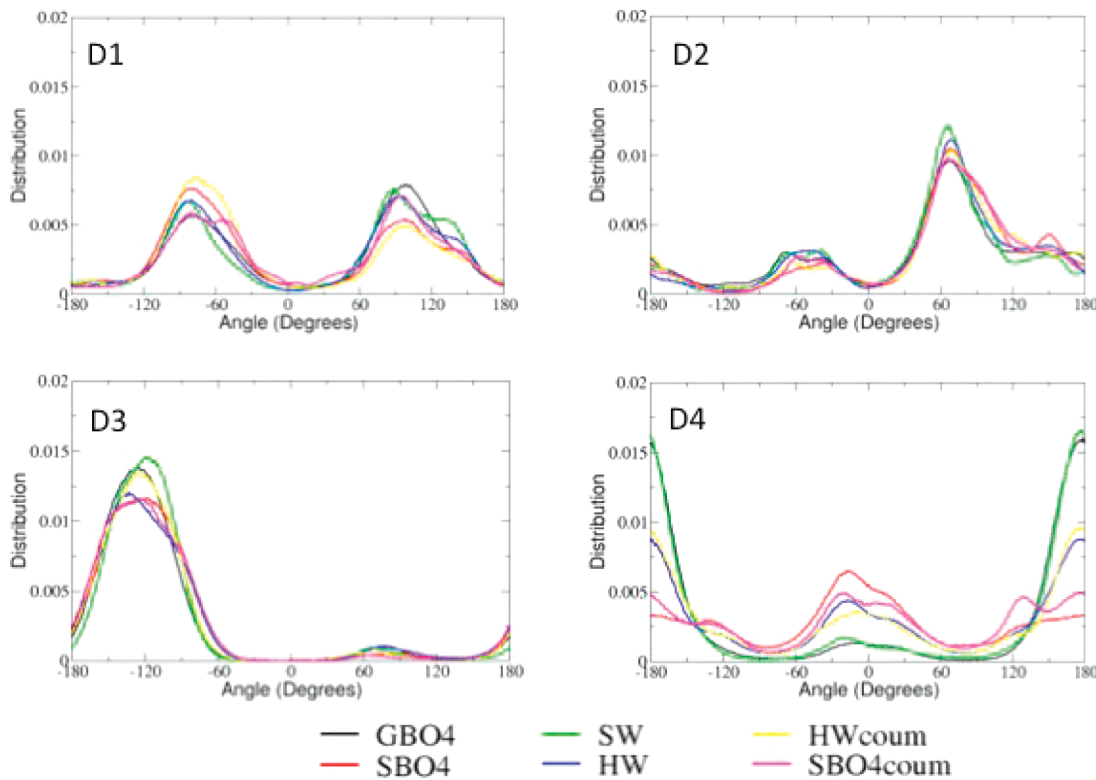


**Figure 6.** Distribution of the four torsion angles D1, D2, D3, and D4 of the  $\beta$ -O-4 linkages.

orientations without discontinuities, whereas very few D3 angles explore a satellite region at  $+g$ . Finally, the torsion angle D4 explores two large angular domains, at  $0^\circ$  and  $180^\circ$ , noting that this angle is substantially sensitive to the nature of the monolignol precursors and, consequently, to the presence or absence of O-Me pendant groups. These results indicate that the four torsion angles simultaneously explore multiple orientations. Thus, in the solid state, lignin possesses a global coil conformation, with the consequence of an overall aperiodic amorphous structure. Our results can be compared with those obtained earlier by Besombes et al.<sup>19,20</sup> The conformational spaces explored by the torsion angles of the  $\beta$ -O-4 linkages of either previously isolated lignin dimers<sup>19,20</sup> or the confined lignin oligomers presented in this study are roughly similar. The small differences observed are not surprising considering that an isolated dimer is not constrained, whereas an oligomer of lignin sandwiched between two surfaces is constrained. Its limited flexibility originates on one hand from the “confinement” effect, which restricts the flexibility of the oligomers of lignin. On the other hand, one has to consider the “oligomer” effect, which is a steric effect induced by the interactions between segments that are distant in the chemical structure but in close proximity in the 3D structure. Indeed, this effect restricts the accessible conformational space of the interunit linkages.

Another important aspect of cell wall lignin deals with the alignment of its chains or its aromatic rings with respect to the cellulose surfaces. These features are illustrated for the system GBO4-a in Figures 7 and 8A and for HWcoum-a in Figure 8B, while all the other systems are reported in Figure S3 of the Supporting Information. Figure 7A is a graphical representation of the skeletons of the two lignin fragments, in red and blue of the model. These skeletons, which do not present any periodicity or any helicity, confirm therefore the dominant

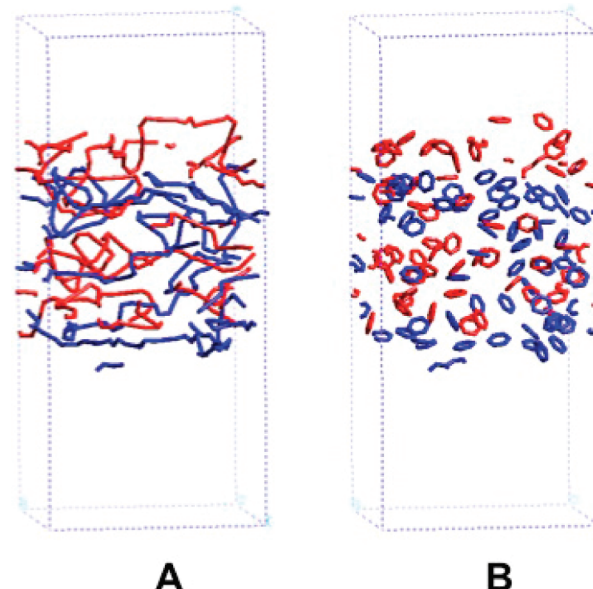


**Figure 7.** Graphical representation of the lignin fraction of the model GBO4-a. (A) Skeleton of the two long lignin fragments (one red and one blue). (B) Aromatic rings of the two lignin fragments. The cellulose layers (not shown) are organized as in Figure 1.

amorphous character of the lignin in this model. In Figure 7B, only the lignin aromatic rings are represented. It appears in this figure that the planes of these rings have various orientations with respect to the surface of the cellulose layers. In fact, when a statistic of these angles is made (Figure 8A), there is a small fraction of these angles that are reflected in the very intense peaks close to  $0^\circ$ , revealing that in this fraction, the aromatic rings of lignin are oriented parallel to the cellulose surface. This

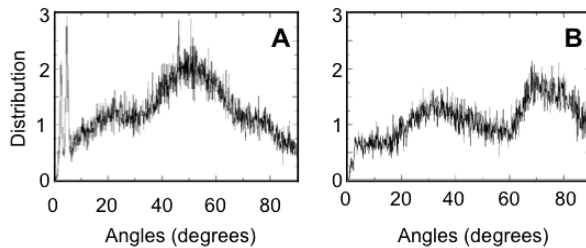


**Figure 8.** Distribution of the angles between the aromatic rings and the plane parallel to the surface of cellulose: (A) in the GBO4-a system; (B) in the HWcoum-a system.

observation is in good agreement with our preceding study.<sup>30</sup> It also fits with the results from Raman<sup>32</sup> or Fourier transform infrared (FT-IR) spectroscopies.<sup>52</sup> Interestingly, the orientation of the aromatic rings of lignin with the cellulose surfaces was found to be model dependent (see Supporting Information, Figure S3). We previously hypothesized<sup>31</sup> that the parallel orientation could be relatively easy to achieve when flexible linkages such as  $\beta$ -O-4 were dominant in the structure (all the a and b models of GBO4, SBO4, and SBO4coum contained only such  $\beta$ -O-4 linkages) and considerably more difficult when less flexible linkages, namely 5-5, 4-O-5, and  $\beta$ -5 were present in the system (all the other models, see the Supporting Information, Figure S1). The present study does not yield reliable evidence to support our earlier hypothesis.

Another aspect of the lignin ultrastructure is the distribution of the angle between the aromatic rings. A survey of these angles as a function of inter-ring distances is illustrated in Figure 9 for two systems, namely, GB04-a and SBO4-a. Despite

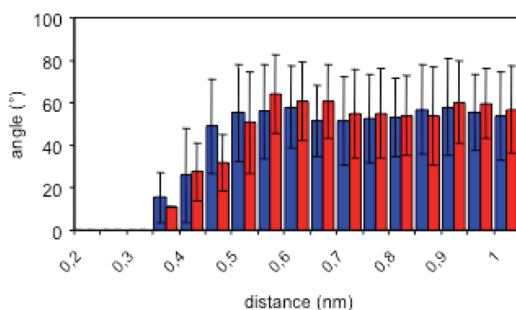


**Figure 9.** Distribution, with error bars, of the angle between aromatic rings as a function of their distance: blue: GBO4-a model; red: SBO4-a model.

the fact that one model (GBO4-a) consists of 100% guaiacyl units and the other (SBO4-a) consists of 100% syringyl units, the distribution of these angles is nearly the same. Locally, at small distances, the aromatic rings are oriented parallel to one another (average angle of less than 20° at 0.35 nm), indicating therefore the existence of a  $\pi$ -stacking. This parallel orientation is obviously lost at large distances where an isotropic distribution of the angle is observed.

The volume of the voids accessible to water molecules is an important feature of the different cell wall models that were investigated. As reported in Table 2, this volume is nearly constant for all models at around 3 nm<sup>3</sup>, i.e., around 4% of the total volume in each model. The number of water molecules within the models is also nearly the same at around 200 for each system, yielding an average occupancy of 0.015 mm<sup>3</sup> per water molecule. From the density profiles observed in Figures 3

and 5, water is distributed exclusively within the xylan and lignin fractions. Even if some water molecules are adsorbed at the cellulose surfaces, none are within the cellulose crystalline phase. Two types of water are identified: isolated molecules that interact strongly with carbohydrates and/or lignin and water aggregates. Whereas the former are nonfreezable water, the latter are able to freeze and, in particular, can be quantified by differential scanning calorimetry (DSC) measurements. The size of the aggregates is particularly heterogeneous and fluctuates with time. Figure 10 illustrates the variability of the

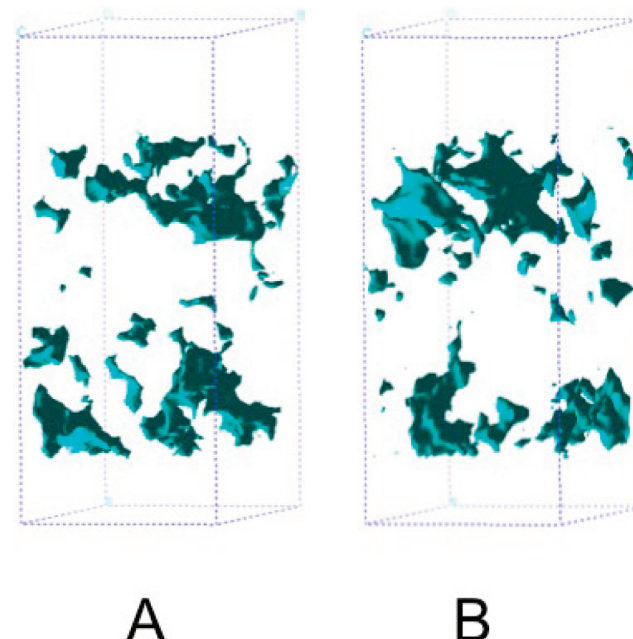


**Figure 10.** Distribution of the volume occupied by water molecules (in green) in (A) the GBO4-a model and (B) the SBO4-b model.

size of the aggregates that could be observed for instance in the models GBO4-a and SBO4-b. Even if the distribution of the void occupied by water appears somewhat different, the overall content is almost the same: 3.17 nm<sup>3</sup> for GBO4-a, and 3.09 nm<sup>3</sup> for SBO4-b.

Other important factors of the hydration of the cell wall model are the diffusion coefficients of the water molecules. The calculation of this diffusion uses Einstein's formalism, where the self-diffusion of water is deduced from the slope of their mean squared displacements (MSDs) versus time. Diffusion coefficients of the water molecules within the different models are given in Table 4. The average diffusion coefficient, estimated from all the models, is  $0.0205 \pm 0.0045 \times 10^{-5}$  cm<sup>2</sup>·s<sup>-1</sup>. We then distinguished the water molecules interacting mostly with lignin and those interacting mostly with the carbohydrate fraction (see the Material and Methods section); their diffusion coefficients are also reported in Table 4. In our case, the mobility of the water molecules in close proximity of lignin is 1.5 times larger than that of carbohydrates. This is in line with the results from NMR data.<sup>5</sup>

The water molecules that are either isolated from the other water molecules or at the frontier of the aggregates participate to the stabilization of the complexes, by interacting not only with lignin but also with the carbohydrates. Each water molecule forms, on average, 2.2 H-bonds with the carbohydrates and only 1.6 with lignins. The models are obviously

Table 4. Diffusion Constants of the Water Molecules ( $\times 10^{-5} \text{ cm}^2 \cdot \text{s}^{-1}$ )<sup>a</sup>

		all water	sd	carbohydrate group	H-bond number per water	lignin group	H-bond number per water
GBO4	a	0.0171	0.0059	0.0019	2.2	0.0087	1.5
	b	0.0243	0.0007	0.0178	2.1	0.0108	1.4
	c	0.0180	0.0042	0.0141	2.2	0.0095	1.6
SBO4	a	0.0178	0.0047	0.0084	2.2	0.0119	1.7
	b	0.0191	0.0076	0.0031	2.2	0.0137	1.4
	c	0.0168	0.0085	0.0057	2.5	0.0118	1.7
SW	a	0.0164	0.0063	0.0056	2.3	0.0220	1.8
	b	0.0259	0.0135	0.0188	2.2	0.0064	1.9
	c	0.0234	0.0141	0.0064	2.1	0.0147	1.6
HW	a	0.0331	0.0129	0.0096	2.3	0.0270	1.3
	b	0.0249	0.0010	0.0067	2.1	0.0298	1.5
	c	0.0171	0.0070	0.0112	2.1	0.0103	1.5
SBO4coum	a	0.0172	0.0069	0.0095	2.1	0.0087	1.6
	b	0.0162	0.0035	0.0073	2.2	0.0099	2.0
	c	0.0189	0.0072	0.0101	2.1	0.0150	1.4
HWcoum	a	0.0222	0.0057	0.0070	2.1	0.0127	1.5
	b	0.0197	0.0034	0.0061	2.6	0.0116	2.0
	c	0.0203	0.0030	0.0048	2.3	0.0130	1.7

<sup>a</sup>The number of H-bonds for each water molecules with either lignin or carbohydrates is also included.

stabilized by weak interactions of the hydrogen bonding type in addition to the  $\pi$ -stacking of the aromatic rings. Details of the hydrogen bonds can be found in Table 3. On average, it is observed that each monolignol residue participates to 1.9 H-bonds, 0.66 of them is intra lignin and 1.24 are between lignin and water. There are only three chemical groups on lignin that can be involved in H-bonds: the hydroxyl, the methoxy, and the ether groups. The former is both a donor and acceptor of hydrogen bonds, and there are only acceptors in the two latter groups. On average, each hydroxyl group in lignin participates in 0.52 H-bonds, while the O-methoxy and O-ether groups participate in only 0.11 and 0.05 H-bonds, respectively. Hydroxyl groups are thus 5 times more involved in hydrogen bonds than the O-methoxy oxygens and 10 times more than backbone O-ether ones.

## DISCUSSION

In this paper, our goal has been to present a stable and versatile molecular model, designed to mimic the composition and organization of the secondary wall of plants and in particular that of grass. As for other lignified plants, this wall presents a redundant layer-like assembly of slender crystalline cellulose microfibrils embedded into a matrix consisting of three other components: hemicellulose, lignin, and water. In view of the wall ultrastructural redundancy, the building of the model could therefore be reduced to the analysis of a periodic box containing cellulose sandwiched by the three matrix components.

It is known that, statistically, the cellulose microfibrils in secondary cell walls of plants are distant from one another by about 4 nm.<sup>53</sup> On the basis of that distance, we could draw the box shown in Figure 1. This box consists of two layers of crystalline cellulose, each being two molecules deep, representing the surface of the microfibrils, separated by the expected interlayer distance around 4 nm thick, and accepting the three other components. In view of its size, the box in Figure 1 and repeated in Figures 3 and 5, accepts  $1.7 \times 10^{-20} \text{ g}$  of xylan and  $3.7 \times 10^{-20} \text{ g}$  of lignin, built on twice more lignin than xylan, whereas water that occupies the leftover voids is only  $0.6 \times 10^{-20} \text{ g}$ , i.e., one-third of the weight of xylan. Thus an estimate

of the overall model is 50% cellulose, 30% lignin, 15% xylan, and 5% water, in line with the current average percentages for lignified plant cell walls.

In this work, the cellulose surface is infinite along the A and C axes of the periodic cell. Periodicity along the chain direction (C axis) is highly desirable, as it allows the modeling of infinite cellulose chains. Two strategies can then be envisaged concerning the periodicity along the dimension A of the cell: the surface along that direction can be modeled either infinite or finite. For the A dimension of the supercell cell, we considered about 3 nm, which is comparable to the lateral dimension of a microfibril in wood. However, the microfibrils are always associated to each other in larger structures called macrofibrils, whose dimensions are typically 15 nm. Macrofibrils can further associate into fibers. Given the typical dimensions of cellulose in wood, we choose to model an infinite surface that, at the scale of atomistic simulations, represents a cellulosic macrofibril. A small adaptation of the procedure allows the modeling of a unique microfibril, which presents a finite surface in the A direction.

In this work, we have investigated only the (110) surface of cellulose. This hydrophilic surface together with that of the corresponding ( $\bar{1}\bar{1}0$ ) is believed to be one of the two dominant surfaces of the cellulose microfibrils that are exposed within the cell wall. Nevertheless, since NMR data have shown that the (110) surfaces has stronger affinity for xylan than its ( $\bar{1}\bar{1}0$ ) counterpart,<sup>54–56</sup> we have restricted our work to only the (110) surface. For cellulose, the choice of representing only the surface chains of a microfibril together with those located just below is justified, as it is known that only the accessible hydroxyl and hydroxymethyl groups of the chains located at the surface of the microfibrils are affected during the dynamics process.<sup>51,56</sup> The underlying chains themselves are essentially frozen into the crystalline lattice and therefore not affected by the MD movements, which modify only the accessible surfaces.

In our final model, most of the xylan molecules are laid flat on the cellulose surface, where locally they can reach a density close to  $1.5 \text{ g} \cdot \text{cm}^{-3}$  (see Figures 3, 4, and 5). There is no interpenetration of the xylan within the cellulose lattice, and, even if the xylan has adsorbed some of the water molecules, the

density of its hydration is not significantly more abundant than in the lignin part of the model. The co-orientation of most of the xylan on the cellulose surface that results from our modeling confirms the experimental observations deduced from either polarized infrared data<sup>57–60</sup> or from ultrastructural observations,<sup>6</sup> as in both cases, the alignment of xylan molecules with respect to the cell wall layers has been reported. Another aspect of the xylan distribution in the model is that xylan displays some interpenetration into the lignin part (Figures 3 and 5). This feature must be partly due to the chemical linkage that has been established between these two components through the ferulate bond. Nevertheless, there are only a few of these bridges, and thus most of the interpenetration must take its origin in the affinity of xylan for lignin. It is interesting to see that the penetration of xylan into the lignin phase is systematically presented in the cell wall models drawn by several authors who have stressed, as we do, the intermediate behavior of xylan between the otherwise incompatible cellulose and lignin cell wall components.<sup>5,6</sup>

When surveying the density profile of our 18 models (see their description in Figure S2 of the Supporting Information), one is struck by the diversity in the local packing of the lignin components, when going from one model to the other. Indeed, locally, we see that the lignin density can vary from 0.5 to 2 g·cm<sup>-3</sup> by just modifying some organizational parameters. Such density variation is exemplified in Figure 5 for the GBO-4 model, where the choice of either long, short, or branched lignin chains, built from the same lignin basic units, leads to lignin density profiles that are drastically different. Another aspect of the lignin component of our models is that some of them present an alignment of some of the lignin aromatic rings with respect to the cellulose surface, whereas others do not. This alignment has been evidenced by Raman<sup>32</sup> or FTIR<sup>60</sup> spectroscopy in several wood species, but it is not known at present whether it would be systematically observed in the secondary wall of all plant species or whether it is specific to only a few of them. Whereas the co-orientation of the lignin phenyl rings with respect to cellulose appears to be model dependent, our models show that there is always some alignment of the phenyl rings with respect to one another due to the classical  $\pi$  bonding stacking, which contributes to the inner cohesion of the lignin phase. This cohesion is not only due to the phenyl rings stacking, but also to a series of hydrogen bonds that link the various basic lignin units (see Table 3).

One of the salient features of all our lignin models is that, despite their similarity and differences, all of them are essentially amorphous, and none of them presents any periodic, helical organization. Thus our models contrast with other proposed MD-based models where regular helical lignin systems have been proposed.<sup>35</sup> This difference may be due to the fact that we have used a more elaborate strategy to build the model, successively incorporating the four constituents of the cell wall. Another reason may be that we have used longer dynamics time and therefore reached more stabilized conditions.

The distribution of water throughout the models is another interesting aspect of this study. In Figures 3 and 5 as well as in the graphs presented in the Supporting Information (Figure S2), the density attributed to water varies from around 0.1 to 0.3 g·cm<sup>-3</sup> and, as expected, there is no water within the cellulose domains. In addition, and as seen in Table 2, the global amount of water within the models, which amounts to

around 200 molecules, appears not to be model-dependent. Besides that observation, it is remarkable that the water density seems to be similar within the xylan and the lignin parts of the system. Despite this similarity, the mobility of water molecules present in the lignin phase is 50% greater than that of the water molecules associated with xylan (Tables 4 and 5). An

**Table 5. Averaged Diffusion Coefficients of the Water Molecules ( $\times 10^{-5}$  cm<sup>2</sup>·s<sup>-1</sup>)**

	diffusion coefficients	sd	N H-bonds/water
all water	0.020466	0.00645	
W carbohydrate	0.008675	0.007058	2.20
W lignin	0.014413	0.005977	1.60

alternative explanation for the different mobility of water within the wood cell wall has been proposed by Hill et al.<sup>5</sup> For these authors, some of the water molecules with a low mobility are believed to be located in a continuous layer at the interface of cellulose and hemicellulose, whereas others of high mobility are distributed throughout the bulk of the cell wall. In the present work, we did not consider any layer of water at the xylan/cellulose interface, but instead our model showed water molecules of different mobility, in relation with their close environment: either polysaccharide or polyaromatic.

Our approach to the building of the lignocellulosic cell wall has been sequential, with the successive addition of cellulose, hemicellulose, lignin, and finally water. It could be that modifying this order of addition would bring some modifications to the model. The interest of our approach is that our computing protocol is quite versatile and robust. It could be used if, for instance, the lignin had been added first and the xylan later or the water first and then the xylan, and so forth. Another modification that could easily be imagined would be to swap glucomannan for xylan or even to have both xylan and glucomannan in the model. This last hemicellulose, which is present in most softwood species, is interesting as it has a better affinity for cellulose than xylan<sup>61</sup> due to its propensity to form 2-fold helices<sup>62,63</sup> compatible with the repeat of crystalline cellulose as opposed to the 3-fold system of xylan.<sup>64</sup>

In this study we have attempted to build a series of reasonable molecular models of the lignified plant cell wall, keeping the cellulose and hemicellulose constant, but using a wide variety of lignin chemistry, ranging from high to low DP, linear to branched molecules, variable H, S, and G composition and, in some cases, the presence of coumaryl units. In addition, even if most of our lignin models contained a high percentage of  $\beta$ -O4 linkages, various proportions of five other types of linkages have also been tested. Despite all these variations, the basic properties resulting from these models do not present substantial diversity.

The modeling technique that has been described here should be very useful to complement studies designed to decipher the important events of the life of the lignocellulosic materials, ranging from their biosynthesis, to their utilization in various industries, to their biodegradation. At present, there is great hope for the use of lignocellulosics for the development of second-generation biofuels. No doubt that modeling will be used to optimize the successive steps that convert such solid biomass into liquid fuel.

## ■ ASSOCIATED CONTENT

### § Supporting Information

The chemical structures (the sequence of monomers and the interunit linkages) of the different lignin considered in this study are given in Figure S1; the density profiles of each modeled system are given in Figure S2; the distributions of the angle between the aromatic rings of lignin and the surface of cellulose of each modeled system are given in Figure S3; the distribution of the angle between aromatic rings of lignin as a function of their distance are given in Figure S4. This information is available free of charge via the Internet at <http://pubs.acs.org>

## ■ AUTHOR INFORMATION

### Corresponding Author

\*E-mail: karim.mazeau@cermav.cnrs.fr; fax: +33 476 03 76 04.

### Notes

The authors declare no competing financial interest.

## ■ ACKNOWLEDGMENTS

This work was partially financed by the ANR Grant MAGIC ANR-08-BLAN0307-01. The authors acknowledge the help of Dr. H. Chanzy for valuable comments during the writing of this work.

## ■ REFERENCES

- (1) Naik, S. N.; Goud, V. V.; Rout, P. K.; Dalai, A. K. *Renewable Sustainable Energy Rev.* **2010**, *14*, 578–597.
- (2) Pauly, M.; Keegstra, K. *Plant J.* **2008**, *54*, 559–568.
- (3) Ruel, K.; Barnoud, F.; Goring, D. A. I. *Wood Sci. Technol.* **1978**, *12*, 287–291.
- (4) Bidlack, J.; Malone, M.; Benson, R. *Proc. Okla. Acad. Sci.* **1992**, *72*, 51–62.
- (5) Hill, S. J.; Franich, R. A.; Callaghan, P. T.; Newman, R. H. N. Z. *J. For. Sci.* **2009**, *39*, 251–257.
- (6) Terashima, N.; Kitano, K.; Kojima, M.; Yoshida, M.; Yamamoto, H.; Westermark, U. *J. Wood Sci.* **2009**, *55*, 409–416.
- (7) Salmén, L.; Burgert, I. *Holzforschung* **2009**, *63*, 121–129.
- (8) Lawoko, M.; Henriksson, G.; Gellerstedt, G. *Holzforschung* **2006**, *60*, 162–165.
- (9) Boerjan, W.; Ralph, J.; Baucher, M. *Annu. Rev. Plant Biol.* **2003**, *54*, 519–546.
- (10) Davison, B. H.; Drescher, S. R.; Tuskan, G. A.; Davis, M. F.; Nghiem, N. P. *Appl. Biochem. Biotechnol.* **2006**, *129*, 427–435.
- (11) Studer, M.; DeMartini, J. D.; Davis, M. F.; Sykes, R. W.; Davison, B.; Keller, M.; Tuskan, G. A.; Wyman, C. E. *Proc. Natl. Acad. Sci. U.S.A.* **2011**, *108*, 6300–6305.
- (12) Bernard-Vailhé, M.-A.; Cornu, A.; Robert, D.; Maillot, M.-P.; Besle, J.-M. *J. Agric. Food Chem.* **1996**, *44*, 1164–1169.
- (13) Baucher, M.; Bernard-Vailhé, M.-A.; Chabberts, B.; Besle, J.-M.; Opsomer, C.; Van Montagu, M.; Botterman, J. *Plant Mol. Biol.* **1999**, *39*, 437–447.
- (14) Goujon, T.; Ferret, V.; Mila, I.; Pollet, B.; Ruel, K.; Burlat, V.; Joseleau, J.-P.; Barrière, Y.; Lapierre, C.; Jouanin, L. *Planta* **2003**, *217*, 218–228.
- (15) Méchin, V.; Argillier, O.; Menanteau, V.; Barrière, Y.; Mila, I.; Pollet, B.; Lapierre, C. *J. Sci. Food Agric.* **2000**, *80*, 574–580.
- (16) Zhang, Y.; Culhaoglu, T.; Pollet, B.; Melin, C.; Denoue, D.; Barrière, Y.; Baumberger, S.; Méchin, V. *J. Agric. Food Chem.* **2011**, *59*, 10129–10135.
- (17) Simon, J. P.; Eriksson, K-E. L. *J. Mol. Struct.* **1996**, *384*, 1–7.
- (18) Petridis, L.; Smith, J. C. *J. Comput. Chem.* **2009**, *30*, 457–467.
- (19) Besombes, S.; Robert, D.; Utile, J.-P.; Taravel, F. R.; Mazeau, K. *J. Agric. Food Chem.* **2003**, *51*, 34–42.
- (20) Besombes, S.; Robert, D.; Utile, J.-P.; Taravel, F. R.; Mazeau, K. *Holzforschung* **2003**, *57*, 266–274.
- (21) Langer, V.; Lundquist, K.; Parkås, J. *BioResources* **2007**, *2*, 590–597.
- (22) Lundquist, K.; Langer, V.; Parkås, J. *BioResources* **2009**, *4*, 529–536.
- (23) Besombes, S.; Mazeau, K. *Biopolymers* **2004**, *73*, 301–315.
- (24) Brunow, G.; Karhunen, P.; Lundquist, K.; Olson, S.; Stomberg, R. *J. Chem. Crystallogr.* **1995**, *25*, 1–10.
- (25) Graver, T. M.; Maa, K. J.; Marat, K. *Can. J. Chem.* **1996**, *74*, 173–184.
- (26) Besombes, S.; Utile, J.-P.; Mazeau, K.; Robert, D.; Taravel, F. R. *Magn. Reson. Chem.* **2004**, *42*, 337–347.
- (27) Petridis, L.; Schulz, R.; Smith, J. C. *J. Am. Chem. Soc.* **2011**, *133*, 20277–20287.
- (28) Houtman, C. J.; Atalla, R. H. *J. Plant Physiol.* **1995**, *107*, 977–984.
- (29) Micic, M.; Radotic, K.; Jeremic, M.; Leblanc, R. M. *Macromol. Biosci.* **2003**, *3*, 100–106.
- (30) Besombes, S.; Mazeau, K. *Plant Physiol. Biochem.* **2005**, *43*, 277–286.
- (31) Besombes, S.; Mazeau, K. *Plant Physiol. Biochem.* **2005**, *43*, 299–308.
- (32) Atalla, R. H.; Agarwall, U. P. *Science* **1985**, *227*, 636–638.
- (33) Vu, T.; Chaffee, A.; Yarovsky, I. *Mol. Simulat.* **2002**, *28*, 981–991.
- (34) Zhang, X.; Yang, W.; Blasiak, W. *Energ. Fuel* **2011**, *25*, 4786–4795.
- (35) Faulon, J.-L.; Carlson, G. A.; Hatcher, P. G. *Org. Geochem.* **1994**, *21*, 1169–1179.
- (36) Mazeau, K. *Carbohydr. Polym.* **2011**, *84*, 524–532.
- (37) Hess, B.; Kutzner, C.; van der Spoel, D.; Lindahl, E. *J. Chem. Theory Comput.* **2008**, *4*, 435–447.
- (38) Nishiyama, Y.; Langan, P.; Chanzy, H. *J. Am. Chem. Soc.* **2002**, *124*, 9074–9082.
- (39) Mazeau, K. *Cellulose* **2005**, *12*, 339–349.
- (40) Fauré, R.; Courtin, C. M.; Delcour, J. A.; Dumon, C.; Faulds, C. B.; Fincher, G. B.; Fort, S.; Fry, S. C.; Halila, S.; Kabel, M. A.; Pouvreau, L.; Quemener, B.; Rivet, A.; Saulnier, L.; Schols, H. A.; Driguez, H.; O'Donohue, M. J. *Aust. J. Chem.* **2009**, *62*, 533–537.
- (41) Mazeau, K.; Charlier, L. *Cellulose* **2012**, *19*, 337–349.
- (42) Mazeau, K.; Moine, C.; Krausz, P.; Gloaguen, V. *Carbohydr. Res.* **2005**, *340*, 2752–2760.
- (43) Ralph, J.; Brunow, G.; Boerjan, W. Lignins. In *Encyclopedia of Life Sciences*; John Wiley & Sons Ltd: Chichester, U.K., 2007; <http://www.els.net> [doi:10.1002/9780470015902.a0020104]
- (44) Henao, L. J.; Mazeau, K. *Mater. Sci. Eng. C* **2009**, *29*, 2326–2332.
- (45) Berendsen, H. J. C.; Postma, J. P. M.; Van Gunsteren, W. F.; Hermans, J. *Jerusalem Symp. Quantum Chem. Biochem.* **1981**, *14*, 331–342.
- (46) Oostenbrink, C.; Villa, A.; Mark, A. E.; Van Gunsteren, W. F. *J. Comput. Chem.* **2004**, *25*, 1656–1676.
- (47) Berendsen, H. J. C.; Postma, J. P. M.; Van Gunsteren, W. F.; DiNola, A.; Haak, J. R. *J. Chem. Phys.* **1984**, *81*, 3684–3690.
- (48) Bussi, G.; Donadio, D.; Parrinello, M. *J. Chem. Phys.* **2007**, *126*, 014101/1–014101/7.
- (49) Darden, T.; York, D.; Pedersen, L. *J. Chem. Phys.* **1993**, *98*, 10089–10092.
- (50) Essmann, U.; Perera, L.; Berkowitz, M. L.; Darden, T.; Lee, H.; Pedersen, L. *G. J. Chem. Phys.* **1995**, *103*, 8577–8593.
- (51) Chauve, G.; Heux, L.; Arouni, R.; Mazeau, K. *Biomacromolecules* **2005**, *6*, 2025–2031.
- (52) Åkerblom, M.; Salmén, L. *Holzforschung* **2003**, *57*, 459–465.
- (53) Jakob, H. F.; Tschech, S. E.; Fratzl, P. *Macromolecules* **1996**, *29*, 8435–8440.
- (54) Larsson, P. T.; Hult, E.-L.; Wickholm, K.; Pettersson, E.; Iversen, T. *Solid State Nucl. Magn. Reson.* **1999**, *15*, 31–40.
- (55) Larsson, P. T. In *Hemicelluloses: Science and Technology*; Gatenholm, P., Tenkanen, M., Eds.; ACS Symposium Series; American Chemical Society: Washington, DC, 2002; Vol. 864, pp 254–268.

- (56) Bergenstråhlé, M.; Wohlert, J.; Larsson, P. T.; Mazeau, K.; Berglund, L. A. *J. Phys. Chem. B* **2008**, *112*, 2590–2595.
- (57) Marchessault, R. H.; Liang, C. Y. *J. Polym. Sci.* **1962**, *59*, 357–378.
- (58) Stevanic, J. S.; Salmén, L. *Holzforschung* **2009**, *63*, 497–503.
- (59) Olsson, A.-M.; Bjurhager, I.; Gerber, L.; Sundberg, B.; Salmén, L. *Planta* **2011**, *233*, 1277–1286.
- (60) Simonović, J.; Stevanic, J.; Djikanović, D.; Salmén, L.; K. Radotić, K. *Cellulose* **2011**, *18*, 1433–1440.
- (61) Tokoh, C.; Takabe, K.; Sugiyama, J.; Fujita, M. *Cellulose* **2002**, *9*, 351–360.
- (62) Ogawa, K.; Yui, T.; Mizuno, T. *Agric. Biol. Chem.* **1991**, *55*, 2105–2111.
- (63) Millane, R. P.; Hendrixson, T. L. *Carbohydr. Polym.* **1994**, *25*, 245–251.
- (64) Nieduszynski, I.; Marchessault, R. H. *Nature* **1971**, *232*, 46–47.